State-dependence of Cenozoic thermal extremes

B. B. Cael[1]* and Philip Goodwin[2]

[1]National Oceanography Centre, Southampton, UK [2]University of Southampton, UK

This paper is a non-peer reviewed preprint submitted to EarthArXiv. This paper is in review at *Nature Communications Earth & Environment*.

State-dependence of Cenozoic thermal extremes

B. B. Cael[1*] and Philip Goodwin[2]

[1]National Oceanography Centre, Southampton, UK
[2]University of Southampton, UK

Oxygen isotopes in sediments reflect Earth's past temperature, revealing a cooling over the Cenozoic punctuated by multimillenial thermal extreme events. These extremes are captured by the generalized extreme value distribution, and the distribution's shape changes with baseline temperature such that large thermal extremes are more likely in warmer climates. Anthropogenic warming has the potential to return the baseline climate state to one where large thermal extremes are more likely.

Analysis of geochemical archives provides insight into Earth's climate history through proxies of paleoclimate conditions (*1*). Characterizing this history is critical for understanding the evolution of modern Earth and for constraining possible future responses to anthropogenic greenhouse gas emissions (*2*). Estimates of cumulative emissions so far, remaining fossil fuel reservoirs and the long-term sensitivity of climate to cumulative emissions (*3, 4*) indicate that humanity has the potential to perturb the climate system enough that the large changes in Earth's paleorecords (*1*) are relevant indicators of its potential response on millennial timescales. It is thus particularly important to determine how paleoclimatic variations may depend on baseline climate state, because this is directly linked to the risk of a large long-term Earth system response to anthropogenic forcing. Variations in Cenozoic climate are studied using deep-sea benthic formaniferal δ^{18}O, which relates approximately inversely to global temperature and linearly to global ice volume such that low δ^{18}O corresponds to warm climate states (*5*). Much of the Cenozoic was a greenhouse climate state with minimal ice volume (*1*), and so δ^{18}O is used as an inverse linear proxy for global temperature (*6*). Analogously, formaninferal δ^{13}C records past carbon cycle changes through isotopic fractionation during photosynthesis. Tremendous scientific effort has gone into producing, refining, and interpreting these records; it is a marvel that we can infer with some confidence so much about Earth's climate tens of millions of years ago based on the isotopic composition of shells of protist algae that sink to and are preserved in the seabed (*7,8*). Figure 1 shows the δ^{18}O record from (*8*) leveraging new methods and measurements, which we focus on here. Four phenomena are evident: i) a long-term cooling trend, ii) the emergence of periodic Pleistocene glacial-interglacial cycles at 2.6 million years ago (Ma), iii) noisy sub-million-year fluctuations before then, and iv) punctuations of the record by large, rapid, negative δ^{18}O excursions corresponding to multimillennial timescale warming events, most notably the Paleocene-Eocene Thermal Maximum (PETM, 56Ma). The long term cooling trend and Pleistocene glacial-interglacial cycles have been the subject of extensive study (*1, 7*), and the sub-million year noise has recently been shown to be consistent with multiplicative fluctuations (*9*), potentially due to metabolic temperature-sensitivity of the biosphere (*10*). The tendency for large negative δ^{18}O excursions, perhaps the most concerning from a future climate perspective, has been noted (*9*), and considerable investigation of individual events such as the PETM shows promise for providing useful constraints on Earth's climate sensitivity (*11*). However, these thermal extreme events (iv) have not been studied quantitatively and collectively, meaning a general explanation for these extremes and their magnitude is lacking, impairing our ability to use these extremes to make inferences about future climate.

The generalized extreme value (GEV) distribution is widely used to study such extremes in other settings (*12*). Analogously to how the ubiquity of normal and log-normal phenomena in

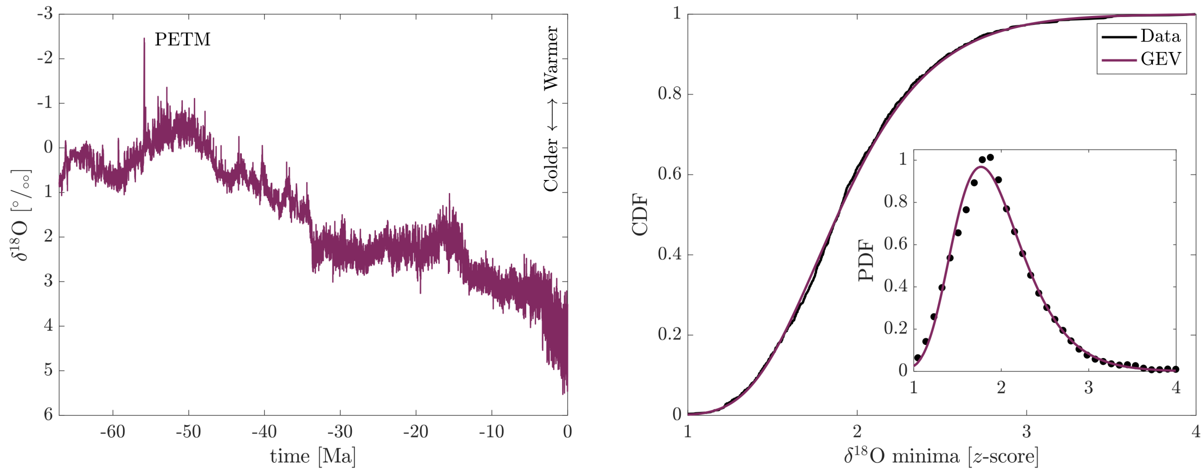

Figure 1: Left: δ^{18}O over the Cenozoic (66Ma-present), from (*8*). Right: Cumulative distribution functions for standardized δ^{18}O block minima and generalized extreme value distribution with maximum-likelihood-estimated parameters. Inset: corresponding probability density functions.

nature is explained by the central limit theorem (*13*), the maxima of many natural phenomena tend to be GEV-distributed, which is explained by the extreme value theorem (Methods). The GEV distribution has three parameters μ, σ, and ξ, the last of which controls the weight of its upper tail (*12*) (Methods). We show that the GEV distribution describes thermal extremes (i.e. δ^{18}O minima) in the Cenozoic excellently, then utilize it to study how the magnitude of these extremes depends on baseline climate state, allowing us to project the increased likelihood of large (>3 standard deviations above baseline) thermal extremes as a function of cumulative emissions.

The distribution of thermal extremes, as captured by standard (z-) scores of δ^{18}O minima in blocks of consecutive δ^{18}O values, is well-characterized as GEV-distributed (Figure 1). The Kolmogorov-Smirnov statistic D quantifies the deviation between the theoretical and empirical distributions; here $D = 0.0213$, well below the threshold $D_{5\%} = 0.0389$ for significance at the 5% level for this sample size (a smaller D-value indicates a better correspondence between the null hypothesis of GEV distribution, and a D-value below $D_{5\%}$ indicates a failure to reject the

GEV distribution at the 5% significance level; Methods). The GEV distribution also applies for δ^{18}O maxima (i.e. thermal minima, $D = 0.0142$), δ^{13}C maxima ($D = 0.0145$), and $\delta^{13}C$ minima ($D = 0.0203$). This result is also robust to choice of block size (Methods). This excellent agreement suggests we can utilize the GEV distribution to characterize the rarity of individual events in terms of return levels and return periods, but more importantly motivates the use of the GEV to investigate the possible dependency of extremes on baseline climate state.

Through this lens of the GEV distribution we investigate whether the magnitude of thermal extremes changes with baseline climate state. We fit the GEV distribution to 'metablocks' of standardized δ^{18}O minima grouped according to their associated mean δ^{18}O values. Figure 2A shows that the shape parameter ξ decreases monotonically as baseline δ^{18}O increases, from $\xi = +0.01 \pm 0.03$ when δ^{18}O = 0±0.5‰, to $\xi = -0.32 \pm 0.08$ when δ^{18}O = 4±0.5‰. The implication of this ξ-change is shown in Figure 2B, which plots the GEV distribution with best-fit parameters for δ^{18}O = 0±0.5 andδ^{18}O = 4±0.5. The relative likelihood of an δ^{18}O minimum $> z$ standard deviations below the mean for a given z-score is captured by the ratio of these distributions' complementary cumulative distribution functions (CCDFs). When δ^{18}O$\sim$4 as over much of the past $\sim$3.5Ma, δ^{18}O minima with z-scores $>$3 are virtually impossible/nonexistent, whereas when δ^{18}O$\sim$0 as at the boundary between the Paleocene and the Eocene, such large excursions still had some probability of occurring. We found no other significant or systematic changes in any other parameters (μ, σ, ξ) of extremes' (maxima/minima of δ^{18}O or δ^{13}C) distributions as a function of baseline climate or carbon cycle state (mean δ^{18}O or δ^{13}C), indicating this phenomenon is restricted to the potential for large thermal maxima depending on the baseline climate state.

As the state-dependency seen in Figure 2A is restricted to thermal maxima and does not materialize in the δ^{13}C record, we interpret it to be driven by state-dependency of the physical climate system, rather than the carbon cycle. Thermal extremes have been interpreted as be-

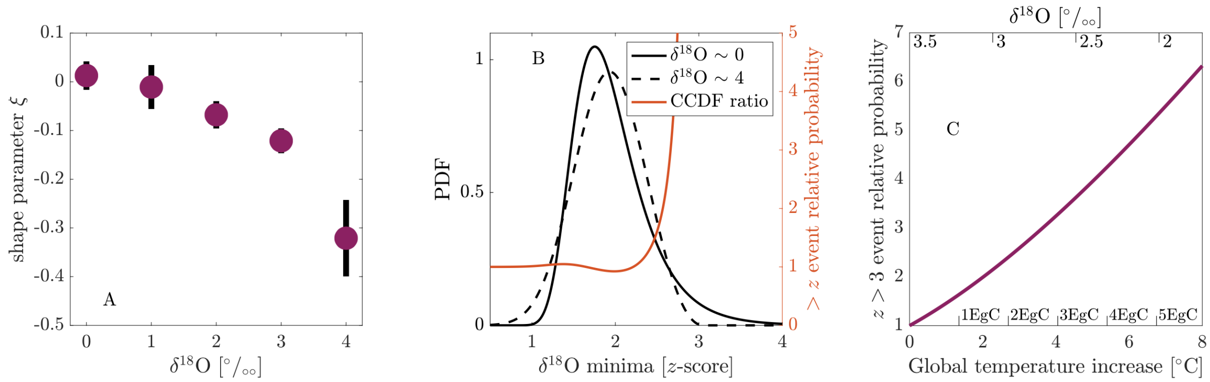

Figure 2: (A) Generalized extreme value (GEV) distribution's shape parameter ξ as a function of baseline climate state. Compare with analogous figures including $\delta^{13}C$ and maxima in δ^{18}O in Fig-S1. (B) GEV probability density function with the parameters from mean δ^{18}O $= 0 \pm 0.5$ (solid black line) and 4 ± 0.5 (dashed black line) from Figure 2A. Orange line is the ratio of these two distributions' complementary cumulative density functions, indicating e.g. that δ^{18}O extremes $>2\frac{2}{3}$ standard deviations below the mean are >3x more likely when δ^{18}O$\sim$0 than when δ^{18}O$\sim$4. (C) Relative likelihood of δ^{18}O extremes >3z (three standard deviations below the mean) for different mean δ^{18}O values (upper x-axis) compared to present (mean δ^{18}O $= 3.5 \pm 0.25$). For instance, such extremes are $\sim$5x more likely when δ^{18}O $= 2 \pm 0.25$.

ing caused by the release of isotopically depleted organic carbon into the surface environment, such as methane hydrates, permafrost, or dissolved organic carbon. Many of these thermal extremes have been shown to be accompanied by extremes in δ^{13}C (*9*). The lack of ξ-changes in δ^{13}C is consistent with a temperature-dependent climate feedback; when the climate is warmer, the same input of carbon produces a larger temperature change (*11*). Temperature-dependent climate feedbacks occur in most Earth System Models, most notably due to the water vapor feedback (*14*) though also possibly due to e.g. ice-albedo or cloud feedbacks. While we cannot exclude the possibility that this dependency is due to carbon cycle perturbations that are balanced in their effect on organic and inorganic carbon and therefore not observed in the $\delta^{13}C$ record, or an external aspect of the Earth system that co-varies with the basline climate state such as silicate weathering, these are less parsimonious explanations given the lack of any relationship involving δ^{13}C extremes and baseline δ^{18}O or vice versa. Additionally, while by any analysis the PETM is an outlier in the δ^{18}O and δ^{13}C record, our results help contextualize it statistically; such a large outlier was far more probable during such a warm climate state, due to the far heavier tail of the thermal extreme distribution.

We can utilize the trend in Figure 2A to estimate Earth's increased susceptibility to large ($>3z$) multimillenial thermal extremes resulting from potential human emissions. As a 0.22‰ change is associated with a $\sim$1°C temperature change (*15*), cumulative carbon emissions so far plus remaining fossil fuel carbon resources are on the order of 5 EgC (= 5 TtC = 5000 PgC = 5000 GtC) (*3*), and 1 EgC cumulative emissions is associated with $\sim$1.35°C long-term warming (*4*), we focus on the δ^{18}O range 3.5($\pm$0.25)-2($\pm$0.25)‰, and estimate the ξ change over the equivalent ranges 3.5-1.75‰ δ^{18}O, 0-8°C temperature anomaly, and 0-6 EgC emissions. The probability of large multimillenial thermal extremes increases with background warming, doubling at approximately 2°C warming, quadrupling at approximately 5°C warming, and sextupling at approximately 7.5°C warming. (These relationships are approximate; this extrapolation should be taken illustratively/qualitatively.)

Altogether our results suggest that thermal extremes over the Cenozoic are more likely to be large when the baseline climate state is warmer. As similar behavior is not seen in carbon cycle extremes, this dependency is most plausibly due to the temperature-sensitivity of physical climate feedbacks. The probability of large multimillenial thermal extremes (superimposed on anthropogenic warming) may considerably increase if a substantial portion of remaining fossil fuel reserves are combusted.

(Word count including abstract, references and figure legends: 1446)

References and Notes

1. Zachos, J., Pagani, M., Sloan, L., Thomas, E. & Billups, K. Trends, rhythms, and aberrations in global climate 65 ma to present. *Science* **292**, 686–693 (2001).

2. Rohling, E. J. *et al.* Comparing climate sensitivity, past and present. *Annual Review of Marine Science* **10**, 261–288 (2018).

3. Rogner, H.-H. An assessment of world hydrocarbon resources. *Annual Review of Energy and the Environment* **22**, 217–262 (1997).

4. Matthews, H. D., Zickfeld, K., Knutti, R. & Allen, M. R. Focus on cumulative emissions, global carbon budgets and the implications for climate mitigation targets. *Environmental Research Letters* **13**, 010201 (2018).

5. Bemis, B. E., Spero, H. J., Bijma, J. & Lea, D. W. Reevaluation of the oxygen isotopic composition of planktonic foraminifera: Experimental results and revised paleotemperature equations. *Paleoceanography* **13**, 150–160 (1998).

6. Hansen, J., Sato, M., Russell, G. & Kharecha, P. Climate sensitivity, sea level and atmospheric carbon dioxide. *Philosophical Transactions of the Royal Society A: Mathematical, Physical and Engineering Sciences* **371**, 20120294 (2013).

7. Emiliani, C. Pleistocene temperatures. *The Journal of geology* **63**, 538–578 (1955).

8. Westerhold, T. *et al.* An astronomically dated record of earth's climate and its predictability over the last 66 million years. *Science* **369**, 1383–1387 (2020).

9. Arnscheidt, C. W. & Rothman, D. H. Asymmetry of extreme cenozoic climate–carbon cycle events. *Science Advances* **7**, eabg6864 (2021).

10. Cael, B., Bisson, K. & Follows, M. J. How have recent temperature changes affected the efficiency of ocean biological carbon export? *Limnology and Oceanography Letters* **2**, 113–118 (2017).

11. Sherwood, S. *et al.* An assessment of earth's climate sensitivity using multiple lines of evidence. *Reviews of Geophysics* **58**, e2019RG000678 (2020).

12. Davison, A. C. & Huser, R. Statistics of extremes. *Annual Review of Statistics and its Application* **2**, 203–235 (2015).

13. Cael, B., Bisson, K. & Follett, C. L. Can rates of ocean primary production and biological carbon export be related through their probability distributions? *Global biogeochemical cycles* **32**, 954–970 (2018).

14. Bloch-Johnson, J. *et al.* Climate sensitivity increases under higher co2 levels due to feedback temperature dependence. *Geophysical Research Letters* **48**, e2020GL089074 (2021).

15. Epstein, S., Buchsbaum, R., Lowenstam, H. A. & Urey, H. C. Revised carbonate-water isotopic temperature scale. *Geological Society of America Bulletin* **64**, 1315–1326 (1953).

16. Stephens, M. A. Edf statistics for goodness of fit and some comparisons. *Journal of the American statistical Association* **69**, 730–737 (1974).

17. Fischer, E., Sippel, S. & Knutti, R. Increasing probability of record-shattering climate extremes. *Nature Climate Change* 1–7 (2021).

Acknowledgments

We thank the many scientists whose collective work has generated the δ^{18}O record which our work investigates, and Manon Duret for comments on a previous draft of this manuscript. Cael acknowledges NERC strategic funding and the Horizon 2020 Framework Programme grant 820989. Goodwin acknowledges NERC grant NE/T010657/1. The work reflects only the authors' view; the European Commission and their executive agency are not responsible for any use that may be made of the information the work contains. Cael conceived the study, performed the analysis, and wrote the paper. Goodwin assisted with analysis and writing. The authors have no competing interests to declare. Data are available from (*8*). Code will be made available at github.com/bbcael and given a DOI via Zenodo should this manuscript be accepted for publication. Reprints and permissions information will be available at www.nature.com/reprints should this manuscript be accepted for publication. Correspondence and requests for materials should be addressed to B. B. Cael (cael@noc.ac.uk).

Online Methods

δ^{18}O records were taken from (*8*) (Figure 1), along with associated δ^{13}C records; these variables and their relationship to temperature and other aspects of the Earth system are described extensively elsewhere. For blocks of consecutive values the mean, standard deviation, and minima were calculated to determine the standard deviations below the mean (z-score) of the minimum δ^{18}O value for that block. The distribution of minima's z-scores is then fit by a generalized extreme value (GEV) distribution via maximum likelihood estimation (Matlab's mle function). The extreme value theorem states that the GEV distribution is the only possible limit distribution of properly normalized maxima of a sequence of independent and identically distributed (i.i.d.) random variables. Natural phenomena are rarely if ever truly i.i.d., but the GEV distribution holds and is applied broadly nonetheless (*12*), analogous to the central limit theorem holding quite accurately for only a handful of summed or multiplied random variables (*13*). The GEV distribution has the form:

$$f(x;\mu,\sigma,\xi) = \frac{1}{\sigma}t(x)^{\xi+1}e^{-t(x)}$$

where $f(\cdot)$ is the probability density function and

$$t(x) = \begin{cases} (1+\xi(\frac{x-\mu}{\sigma}))^{-1/\xi} & \text{if } \xi \neq 0 \\ e^{-(x-\mu)/\sigma} & \text{if } \xi = 0 \end{cases}$$

so μ, and σ are the location and scale parameters and ξ is the parameter that controls the shape of the distribution. Whether the empirical distribution of maxima deviates significantly is then determined by calculating the Kolmogorov-Smirnov statistic D, which is the maximum difference between the hypothesized and empirical cumulative distribution functions, and comparing it to a critical value at the 5% significance level, $D_{5\%}$ (*16*); the difference is not significant if $D < D_{5\%}$. Figure 1 uses the minimum block size of 20 from (*17*), for which $D = 0.0213 < D_{5\%} = 0.0389$ and the median z-score is 1.91. Here we focus on the minimum block size because maximizing the number of blocks is useful to assess changes in the distribution's shape as a function of baseline climate state, as this requires grouping sets of blocks into 'metablocks.' In general, the larger the block size, the larger the minima's z-scores will be, and also the larger $D_{5\%}$ will be due to a smaller sample size of maxima. For instance, using a block size of 67 (the largest prime factor of the length of the δ^{18}O record, 24321) yielded a $D = 0.0279 < 0.0708 = D_{5\%}$ and a median z-score of 2.46, while a block size of 33 (another factor of 24321) yielded $D = 0.0202 < 0.0498 = D_{5\%}$ and a median z-score of 2.17. D-values for δ^{18}O maxima and δ^{13}C maxima and minima reported in the main text are for the same block size of 20, and are also significant for larger block sizes.

Figure 2A was generated by repeating this process on metablocks of block minima, where blocks were grouped by their mean δ^{18}O values into the bins (0,1,2,3,4)±0.5‰. Uncertainties (shown using the robust metric of median absolute deviation) were estimated by bootstrap resampling the distribution of maxima and re-fitting the GEV distribution. We use 10,000 bootstrap iterations, which we find to be more than sufficient as ten 1,000-member subsets were negligibly different. The other GEV distribution parameters (location μ and scale σ) vary negligibly, neither systematically nor significantly ($p \geq 0.33$ for the block and bin sizes in Figure 2A; this also holds for the bin sizes in Figure 2C), with basline climate state (i.e. across metablocks). The decreasing trend of ξ with mean δ^{18}O holds for larger block sizes (e.g. 33 from above) or narrower bin widths (e.g. ±0.25 from Figure 2C. In Figure 2B, the complementary cumulative distribution function of a probability distribution is one minus its cumulative distribution function. For Figure 2C, we repeat the procedure to estimate the δ^{18}O-dependence of ξ (with uncertainties) using the bins (2,2.5,3,3.5)±0.25. We then perform a weighted regression of ξ vs. mean δ^{18}O to estimate $\xi(\delta^{18}\text{O})$ over this range, yielding an estimate of the GEV distribution for any given δ^{18}O value between 1.75-3.5‰. (Note again that other GEV parameters do not change systematically or significantly over this range, or over the entire δ^{18}O range.) This is then used to calculate the probability density >3 z-scores, which is shown in Figure 2C relative to the probability density >3 z-scores estimated for present-day $\delta^{18}\text{O} = 3.5$‰. We underscore that this subfigure, which includes assumed proportionalities between δ^{18}O, global temperature change, and cumulative emissions, should be interpreted as illustrative and qualitative.

We repeated these calculations for block maxima of δ^{18}O and for block maxima and minima of δ^{13}C. All of these were well-characterized by GEV distributions ($D < D_{5\%}$ in each case), but we found no evidence for any state-dependence other than that reported in the main text. In other words only the shape parameter ξ for δ^{18}O minima was dependent on mean δ^{18}O, and no other GEV distribution parameter of any other maxima or minima was dependent on mean δ^{18}O or δ^{18}C.

The glacial-interglacial cycles of the Quaternary period (2.6Ma–present) are recognized not to follow the same sort of fluctuation characteristics as the rest of the Cenozoic, which must be accounted for in any analysis of extremes. Figures 1 and 2 exclude the last 2Ma;

neither increasing this to excluding the entire Quaternary period (2.6Ma) nor decreasing this to excluding only after the mid-Pleistocene transition (1.25Ma) affects the results or conclusions. Additionally, these are robust to including the Quaternary period and filtering out the glacial-interglacial cycles via robust locally estimated scatterplot smoothing (R-LOESS) with a window size of 10. Finally we note that our interpretation of δ^{18}O minima as thermal maxima is robust to effects of ice volume on δ^{18}O because ice sheets primarily act to change the slope and intercept of the linear temperature-δ^{18}O relationship $T \approx \alpha - \beta\delta^{18}$O, with $\alpha, \beta > 0$ approximately constant over the timescales of the extremes considered here. Finally we note that excluding the PETM did not affect our results (as would be expected, as this is only one thermal maximum, and we are analyzing distributions of many thermal maxima) and therefore our inferences about PETM likelihood are not confounded by including it in our analyses.

Supplemental Figure

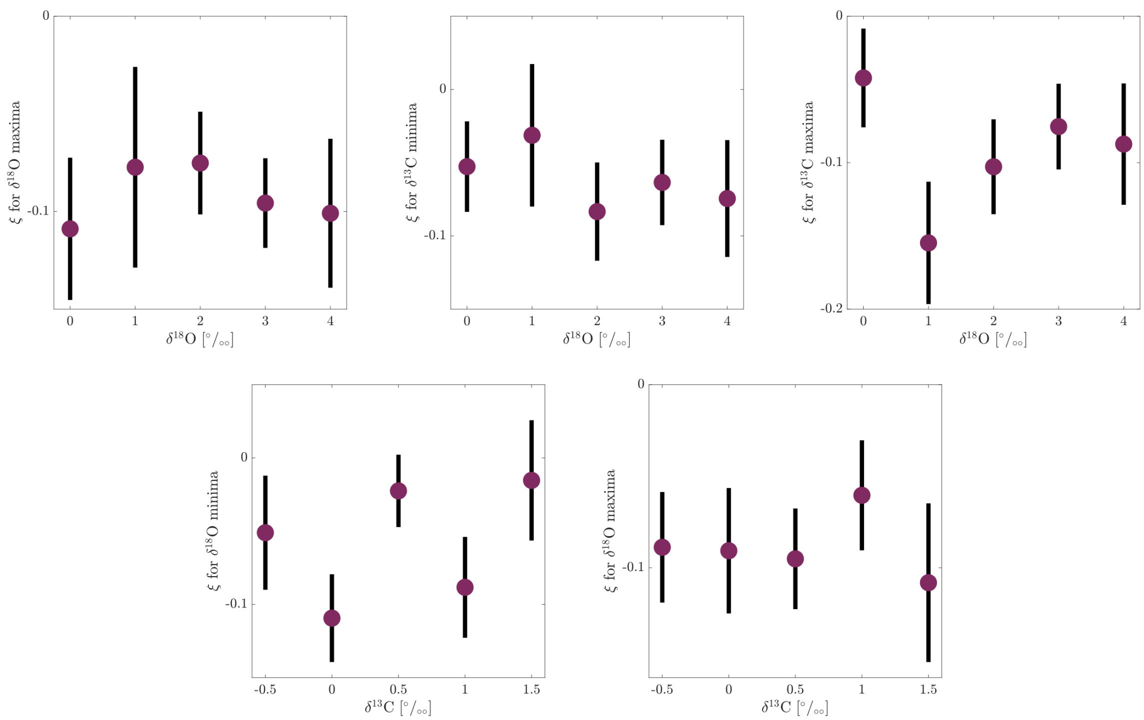

Fig-S1. As Figure 2A but for ξ of maxima in δ^{18}O vs. baseline δ^{18}O, ξ of maxima and minima in δ^{13}C vs. baseline δ^{18}O, and ξ of maxima and minima in δ^{18}O vs. baseline δ^{13}C.